Surface oxides on close-packed surfaces of late transition metals

2006 J. Phys.: Condens. Matter 18 R481

(http://iopscience.iop.org/0953-8984/18/30/R01)

INSTITUTE OF PHYSICS PUBLISHING JOURNAL OF PHYSICS: CONDENSED MATTER

J. Phys.: Condens. Matter **18** (2006) R481–R499 doi:10.1088/0953-8984/18/30/R01

TOPICAL REVIEW

Surface oxides on close-packed surfaces of late transition metals

Edvin Lundgren[1,4], Anders Mikkelsen[1], Jesper N Andersen[1], Georg Kresse[2], Michael Schmid[3] and Peter Varga[3]

[1] Department of Synchrotron Radiation Research, Lund University, Box 118, S-221 00, Lund, Sweden
[2] Institut für Materialphysik and Centre for Computational Materials Science, Universität Wien, A-1090 Wien, Austria
[3] Institut für Allgemeine Physik, Technische Universität Wien, A-1040 Wien, Austria

E-mail: Edvin.lundgren@sljus.lu.se

Received 9 May 2006, in final form 7 June 2006
Published 14 July 2006
Online at stacks.iop.org/JPhysCM/18/R481

Abstract

In recent years, the formation of thin, well-ordered but complex surface oxides on late transition metals has been discovered. The driving force for this line of research has been the strong incentive to increase the partial pressure of oxygen from ultra-high vacuum to conditions more relevant for heterogeneous catalysis. Here we review the present status of the research field. Compared to oxygen adatom superstructures, the structure of the surface oxides has proven to be extremely complex, and the investigations have therefore relied on a combination of several experimental and theoretical techniques. The approach to solving the structures formed on close-packed surfaces of Pd and Rh is presented in some detail. Focusing on the structures found, we show that the surface oxides share some general properties with the corresponding bulk oxides. Nevertheless, of all surface oxide structures known today, only the two-dimensional surface oxides on Pd(100) and Pt(110) have the same lattice as the bulk oxides (PdO and PtO, respectively). In addition to two-dimensional oxides, including the O–Rh–O trilayers found on Rh, one-dimensional oxides were observed at ridges or steps of open surfaces such as (110) or vicinal surfaces. Finally, we briefly report on a few studies of the reactivity of surface oxides with well-known structure.

(Some figures in this article are in colour only in the electronic version)

Contents

[4] Author to whom any correspondence should be addressed.

1. Introduction

Oxidation of metals and semiconductors is of fundamental importance in both solid state physics and chemistry. The oxidation process to a higher or lower degree occurs for all materials, significantly changing the properties from those of the original material. Obtaining a detailed understanding of the atomic-scale processes involved when oxides form as well as of the detailed atomic geometry of the oxide layers formed is therefore an important task in solid state physics and chemistry.

In surface science, a major reason for the interest in oxygen interaction with metal surfaces is heterogeneous catalysis. Using model systems such as low-index single crystal surfaces under ultra-high vacuum (UHV) conditions and carefully controlling the reactant gas abundance on the surface, significant progress has been made in the understanding of adsorbate–adsorbate and adsorbate–substrate interactions [1, 2]. For instance, CO oxidation on transition metal surfaces, which is believed to be an important model systems for oxidation catalysis, has been extensively studied and is at present rather well understood. However, it has recently been realized that it may not be the bare metal surface but rather its oxidized form which is the most active phase under the pressure and temperature conditions appropriate for real-world catalytic oxidation reactions [3–6]. A high partial oxygen pressure is often required in order to form the oxide and consequently typical surface science investigations at lower partial pressures have rather investigated chemisorbed oxygen overlayers than the oxide phases relevant to typical operating conditions of for example metal particle catalysts [7, 8]. Because of these issues, there is a rapid technical development expanding the literature based on *in situ* techniques under realistic conditions [4–6, 9–17]. The understanding which these and future investigations are expected to result in is likely to be highly important for oxidation catalysis on metal nanoparticles, as such particles are expected to oxidize more easily than a macroscopic surface.

In the case of Ru, which is not active in CO oxidation at low O partial pressures but one of the most active catalysts at high oxygen partial pressures [3], the increase in activity can be explained on the atomic scale. The reason is the formation of a thin film of $RuO_2(110)$, resulting in coordinatively unsaturated sites at which impinging CO atoms may adsorb and react with loosely bound bridging O atoms also available at the oxide surface [18]. Thus the increased macroscopic reactivity can be directly linked to the detailed geometry on the microscopic atomic length scale.

The description of the CO oxidation process is more complicated in the case of Pt, Rh, and Pd, one reason being the higher pressures needed for oxide formation so that electron based surface science techniques cannot be used in a traditional fashion. However, the understanding

of the structures formed under more realistic pressure conditions that are insufficient for bulk oxide formation on these metals, so-called surface oxides, has improved significantly during recent years both experimentally and theoretically [13, 19–24]. The role of surface oxides in for instance CO and hydrocarbon oxidation reactions is at present not clear. However, the structural understanding of surface oxides may prove necessary if metal nanoparticles are to be studied under working conditions.

The present review concerns the atomic arrangement of surface oxides formed on late transition metals. In particular, the surface oxides formed on close-packed surfaces on Pd and Rh are presented in some detail. By combining several experimental and theoretical methods, it has been possible to determine the atomic structure of highly complex thin surface oxide films. By first narrowing the choice of candidate structures by the use of qualitative experimental methods such as low-energy electron diffraction (LEED), scanning tunnelling microscopy (STM) and high-resolution core level spectroscopy (HRCLS), density functional theory (DFT) can be efficiently used to calculate the most stable structure among this selection. Finally, these structures can be confirmed or rejected by simulating the experimental results. This approach has led to the general recognition of the existence of surface oxides on late 4d transition metals.

2. Methodology

Below we present the results from structural investigations of the surface oxide formation on Pd(111) [19], Pd(100) [21], Rh(111) [13], and Rh(100) [23]. In each case, we give a short summary of the oxygen-induced structures that have been observed previously and their interpretations. Our results are always presented in the following way. We start using qualitative structural methods such as LEED and STM. This normally gives us a good approximation of the symmetry of the structure and its in-plane lattice distance. Next we discuss HRCLS, which is sensitive to the chemical surrounding of the photoemitting atom, providing the chemical composition in terms of oxygen and transition metal abundances. Using the experimentally obtained symmetry and relative abundances of the species found by HRCLS, a first stable structure can be obtained using DFT [25]. The structural model is then tested by simulating the STM images using a Tersoff–Hamann approach [26] and calculating the core-level binding energies. In the case of Rh(100), the c(8×2) structure was also determined using quantitative LEED and quantitative surface x-ray diffraction (SXRD). Further, if the surface oxide is incommensurate with the substrate and results in a very large unit cell, as in the case of the $\sqrt{6}$ on Pd(111) and the (9×9) on Rh(111), SXRD has been used to determine the exact in-plane lattice distance.

We will now describe the cleaning and preparation procedures. Starting with Pd(100) and Pd(111), the surfaces were cleaned by cycles of Ar^+ sputtering with subsequent annealing to 1100 K and oxygen treatments keeping the samples at 900 K in an oxygen pressure of 2×10^{-8} mbar followed by flashes to 1100 K. The Rh(100) and Rh(111) surfaces were cleaned by cycles of Ar^+ sputtering with subsequent annealing to 1200 K and oxygen treatments keeping the sample at 900 K in an oxygen pressure of 2×10^{-8} mbar followed by flashes to 1200 K. The preparation details of the surface oxides on Pd and Rh surfaces are described in table 1.

3. Surface oxides on Rh and Pd

3.1. Surface oxide on Pd(111): $\sqrt{6}$

Starting with the Pd(111) surface, previous investigations of the oxygen interaction have shown that at a coverage of 0.25 ML a p(2×2) structure exists. A structure at higher O coverages was

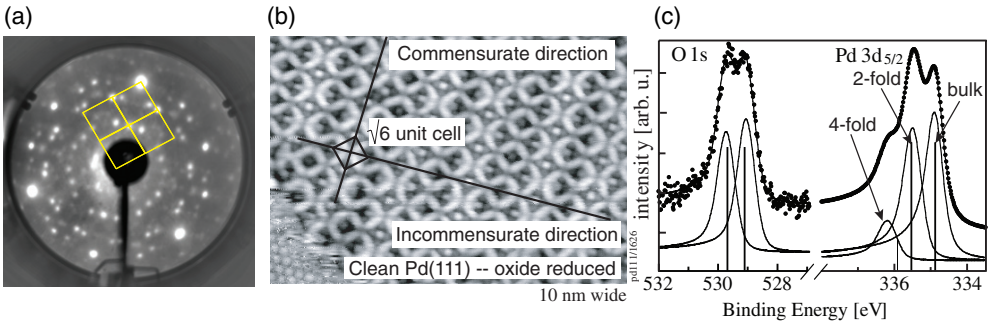

Figure 1. (a) LEED pattern from the Pd(111) surface obtained after 1×10^{-5} mbar O_2 for 600 s at 575 K. (b) STM image of the $\sqrt{6}$ surface oxide on Pd(111). (c) HRCLS from the $\sqrt{6}$ surface oxide on Pd(111). Decomposed experimental spectra as well as calculated core level binding energy shift from the model in figure 2(a) are shown. In the decomposition, the Pd 3p signal has been subtracted from the original spectra.

Table 1. Preparation procedures reported for the surface oxides of Pd and Rh.

Surface	p_{O_2} (mbar)	T (K)	t (s)
Pd(111)-($\sqrt{6}$)	1×10^{-5}	575	600
Pd(100)-($\sqrt{5} \times \sqrt{5}$)R27°	1×10^{-6}	575	600
Rh(111)-(9 × 9)	1×10^{-3}	700	600
Rh(100)-c(8 × 2)	5×10^{-5}	700	600
Rh(110)-c(4 × 2)	1×10^{-4}	750	—

observed by Conrad *et al* [27] and was later studied in more detail by Zheng and Altman [28]. The structure has a square cell with one of its sides corresponding to $\sqrt{6}$ times the nearest-neighbour distance of Pd and we will therefore refer to it as the '$\sqrt{6}$' structure.

In figure 1(a) the LEED pattern after exposing the Pd(111) to 1×10^{-5} mbar O_2 for 600 s at 575 K is shown. The surface cell, which is close to a $\sqrt{6}$ cell, and one of its three domains is indicated. The LEED pattern shows that the structure is commensurate in the $[2\bar{1}\bar{1}]$ direction but incommensurate in the $[0\bar{1}1]$ direction.

In STM, a complex Asian carpet-like structure can be observed; see figure 1(b). It is clear that the appearance is dominated by electronic effects, and the interpretation is therefore not straightforward. By comparison with a p(1 × 1) region visible in the STM image (see figure 1(b)), we can confirm that the side lengths of the indicated squared cell are $\sqrt{6}$, and also that the structure is commensurate in the $[2\bar{1}\bar{1}]$ direction but incommensurate in the $[0\bar{1}1]$ direction. To estimate the number of Pd atoms in the structure, we can remove the oxygen atoms in the structure by reacting it with CO, resulting in a surface with a large number of hexagonal 1 ML (monolayer) deep holes. The reason for the holes is that the Pd atoms in the $\sqrt{6}$ structure has a lower Pd content as compared to that of a Pd(111) plane. By estimating the area of the holes, we find that the $\sqrt{6}$ has a Pd coverage of 0.69 ML, and by taking into account the area of the $\sqrt{6}$ as compared to that of the p(1 × 1), we find that we must place approximately 5 Pd atoms in the $\sqrt{6}$ cell, presumably at the bright protrusions observed by STM.

In HRCLS, two components in the O 1s spectrum and a strongly shifted Pd $3d_{5/2}$ component in the Pd $3d_{5/2}$ region can be observed; see figure 1(c). These observations directly indicate that a strongly intermixed O–Pd layer is present on the surface. The O coverage in the $\sqrt{6}$ can be estimated to be approximately 0.7 ML based on a calibration with the (2 × 2)

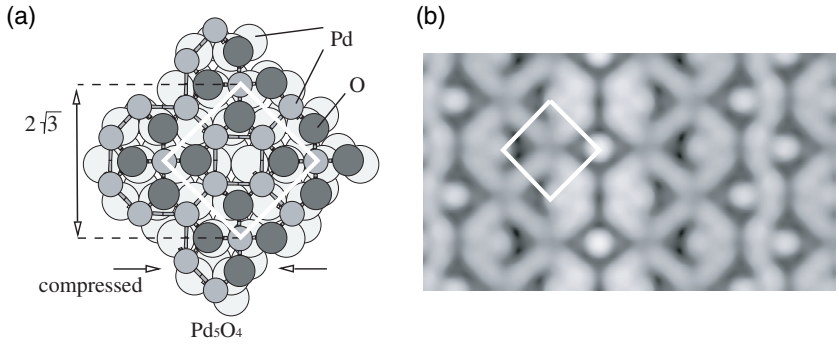

Figure 2. (a) The $\sqrt{6}$ structure as obtained by DFT and simulated annealing on a modified substrate [19]. (b) Simulated STM image of the structure according to the model in (a).

structure at a coverage of 0.25 ML. Therefore, it was found that, being cautious concerning the intensity calibration, 4–6 O atoms should be placed in the $\sqrt{6}$ cell. The O 1s components have a ratio of 1:1, while the two components at 335.6 and 336.1 eV in the Pd $3d_{5/2}$ level have a ratio of approximately 1:4. This leads us to the conclusion that the model must consist of two distinctly different O atoms with equal amounts, and of two distinctly different Pd atoms with a ratio of 1:4.

At this stage one may try to place the exact location of the O and Pd atoms within the $\sqrt{6}$ unit cell, by using simulated annealing based on DFT [25]. Three models were calculated, all of them with the Pd atoms in the locations where the STM image show bright protrusions. In these models, 4, 5, or 6 oxygen atoms were placed within the $\sqrt{6}$ structure, and simulated annealing based *ab initio* DFT calculations were performed for each of the models. Apart from some geometrical restraints due to the incommensurability of the structure, the global energy minima of Pd_5O_4, Pd_5O_5 and Pd_5O_6 adsorbate layers were found by first melting the adsorbate layers at 3000 K, then cooling them in 20 ps (20000 time steps) to 1000 K, and finally quenching each annealed structure into the nearest local energy minimum. Of the three simulated compositions only the final Pd_5O_4 structure had a larger oxygen adsorption energy than bulk PdO or a hypothetical $p(2 \times 1)$ oxygen overlayer with 0.5 ML coverage. This is a prerequisite for the formation of the surface oxide, however, since otherwise the $p(2 \times 1)$ oxygen overlayer or bulk PdO would form at higher oxygen coverage. Such a $p(2 \times 1)$ has not been observed in experiments, however.

The final structure [19] found by the simulated annealing calculations is shown in figure 2(a), and can now be tested by the experimental results. Starting with the STM image, only the Pd_5O_4 structure can reproduce the experimental image as can be seen in figure 2(b). Further, by calculating the core level binding energies from the Pd_5O_4 structure, a good agreement between the calculations and the experimental results is found. The two components in the Pd $3d_{5/2}$ core level are due to two-fold and four-fold O coordinated Pd atoms, respectively. The two O components are due to two different Pd coordinated O atoms, in particular due to a difference in the O coordination to the Pd interface layer. The calculated core level binding energies are indicated in figure 1(c) and the agreement is not perfect, but satisfactory. It should be noted that small shifts in the core level binding, due to differences in the surroundings due to the incommensurability of the structure with the substrate, can be seen as a contribution to the width of the core level.

Finally, the Pd_5O_4 structure could be confirmed by the use of SXRD. In particular the Pd_5O_5 structure could be tested by introducing an additional O atom, which resulted in a

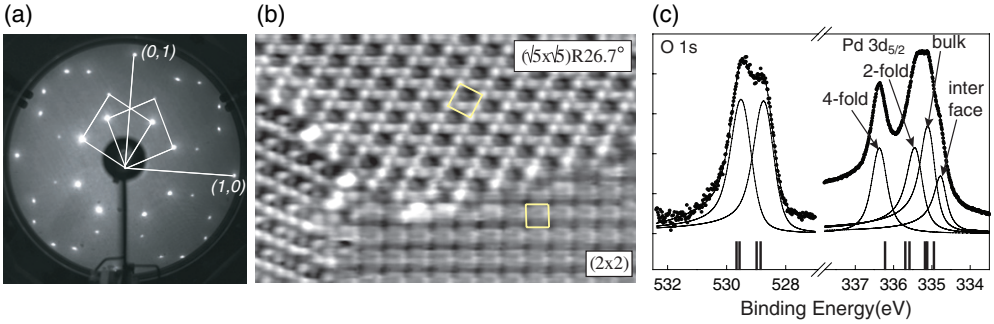

Figure 3. (a) LEED pattern after exposing the Pd(100) surface to 1×10^{-6} mbar O_2 at 575 K for 600 s, displaying a $(\sqrt{5} \times \sqrt{5})$R27° structure. (b) STM image (60 Å wide, $I = 0.67$ nA, $V = 0.76$) from an area of the $(\sqrt{5} \times \sqrt{5})$R27° displaying two domains as well as a patch of the $p(2 \times 2)$. Note that adjacent rows in the $(\sqrt{5} \times \sqrt{5})$R27° are shifted with respect to each other. (c) HRCLS from the $(\sqrt{5} \times \sqrt{5})$R27°; note the two components in the O 1s signal. In the O 1s spectrum, the Pd 3p contribution has been subtracted. The straight lines indicate calculated core level binding energies according to the model in figure 4(a).

significantly worse fit, ruling out this model. It is important to note that the surface oxide binds to the substrate via O on top of or on bridge sites on the Pd(111). It should also be noted that, even though the $\sqrt{6}$ is the most common surface oxide on the Pd(111) surface, surface oxides with other arrangements have been observed [28, 29]. Recent results indicate an even larger number of metastable surface oxides on Pd(111) than reported so far. Most of these structures contain elements of both the $\sqrt{6}$ and the $(\sqrt{5} \times \sqrt{5})$R27° observed on Pd(100) [30].

3.2. Surface oxide on Pd(100): $(\sqrt{5} \times \sqrt{5})R27°$

The initial oxidation of Pd(100) results in four ordered surface structures [31–35]: $p(2 \times 2)$, $c(2 \times 2)$, (5×5) and a $(\sqrt{5} \times \sqrt{5})$R27°. In the case of the low-coverage structures $p(2 \times 2)$ and $c(2 \times 2)$, no indication of the formation of an ordered surface oxide has been reported. Instead, a more simple adsorption behaviour has been observed: the oxygen atoms have been assigned to adsorb in four-fold hollow sites with a coverage of 0.25 and 0.5 ML, respectively [31, 32, 36]. More interestingly, previous studies of the structures with higher oxygen coverage point towards the formation of a surface oxide.

The surface oxide on Pd(100) displays a $(\sqrt{5} \times \sqrt{5})$R27° structure with two domains in LEED; see figure 3(a). The LEED pattern can be interpreted as a square lattice stacked on top of the square substrate lattice, which was done previously using a single plane of PdO(001) as the layer on top of the Pd(100) surface layer as proposed by Orent and Bader [31]. Later, it was thought that this model was confirmed, and quantitative LEED measurements preferred the formation of a single PdO(001) plane with an oxygen content of 0.8 ML as the structural arrangement [37, 38].

In figure 3(b) we show an STM image from two of the domains of the $(\sqrt{5} \times \sqrt{5})$R27° as well as an area with the $p(2 \times 2)$ structure. By assuming that the depressions in the $p(2 \times 2)$ correspond to O in four-fold hollow sites, a Pd(100) lattice can be constructed. Using this lattice, it can be shown that the depressions in the $(\sqrt{5} \times \sqrt{5})$R27° correspond to Pd atoms in hollow sites. It can also be seen that the rows in the $(\sqrt{5} \times \sqrt{5})$R27° structure are shifted half a Pd nearest neighbour distance with respect to the adjacent rows. These observations cannot be explained by the original model. Instead, one might consider a model based on the PdO(100) plane [21].

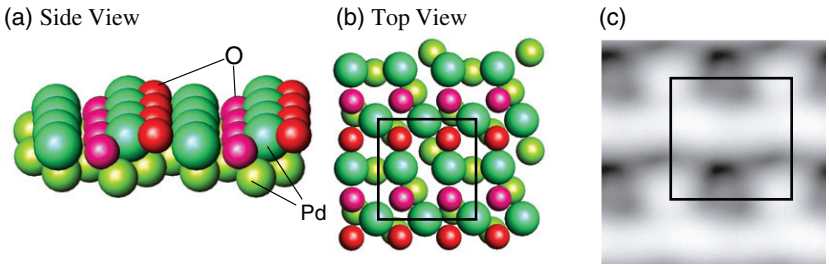

Figure 4. (a) Side view and (b) top view of the PdO(101) model of the $(\sqrt{5} \times \sqrt{5})$R27° structure based on the PdO(101) plane. (c) Simulated STM image using the $(\sqrt{5} \times \sqrt{5})$R27° structure.

In figure 3(c) we show the HRCL spectra of O 1s and Pd $3d_{5/2}$ from the $(\sqrt{5} \times \sqrt{5})$R27° structure. Two components can be observed in the O 1s region, strongly suggesting the existence of two distinctly different O species in the $(\sqrt{5} \times \sqrt{5})$R27° structure. This immediately puts the correctness of both the LEED and the STM models presented above under some serious doubts, since in both models only one type of O is present. Further, in the Pd $3d_{5/2}$, four components can be seen after decomposition, the Pd bulk component, one component that is related to the Pd atoms at the interface between the Pd surface and the surface oxide, and two components due to lower and higher O coordinated Pd in the surface oxide film. Concerning the O coverage, this can be estimated from the O 1s core level by comparing to lower coverage structures to be 0.8 ML, in good agreement with previous studies. The ratio between the two O components is 1:1, indicating an equal amount of the two different oxygen species present on the surface. The relative Pd content of the two oxygen-induced Pd components is also found to be 1:1.

By DFT calculations, a new model can be obtained, as shown in figure 4(a), which can be described as a strained layer of Pd(101) on top of the Pd(001) surface, or a so-called O–Pd–O trilayer [21]. In this model, the two O 1s components are intuitively understood since half of the oxygen atoms are below the surface while the other half are at the surface. Further, half of the Pd atoms are coordinated to two oxygens, while the other half are coordinated to four, explaining the observed shifts in the Pd $3d_{5/2}$ level. A more recent computational study using simulated annealing results in essentially the same structure, but with a slight in-plane shift with respect to the substrate. This structure was recently confirmed by a quantitative LEED study [39].

In figure 4(a) the PdO(101) model of the $(\sqrt{5} \times \sqrt{5})$R27° structure is shown. One way to confirm that the PdO(101) structure is the correct structure is to simulate the experimental STM images using the Tersoff–Haman approach. A comparison between experiment and theory is given by figures 3(b) and 4(c). In particular, the dark appearance of the Pd atom situated in the hollow site is reproduced by the simulation.

Additional confirmation can be obtained by comparing the calculated core level binding energy shifts with the experimental shifts shown in figure 3(c). Only the PdO(101) model reproduces the two components in the O 1s level and the three oxygen-induced components in the Pd $3d_{5/2}$ level, giving us confidence in the model.

3.3. Surface oxide on Rh(111): (9 × 9)

On Rh(111) a number of oxygen-induced structures are produced with increasing O coverage. Some of these structures have been studied in detail by various groups, in particular the p(2 × 2)

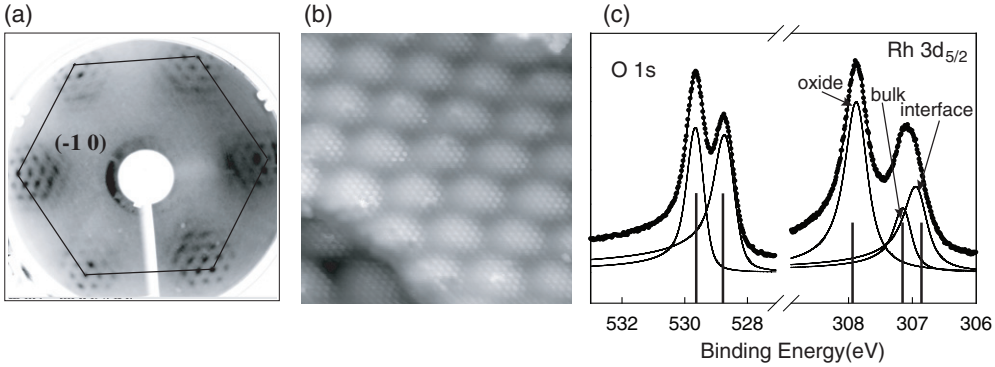

Figure 5. (a) LEED pattern obtained after exposing the RH(111) surface to an O_2 partial pressure of 1×10^{-3} mbar at 700 K. The hexagon indicates the integer order LEED spots from the Rh(111) substrate. (b) STM image from the (9×9) on Rh(111) (-4 mV 0.5 nA, 100 Å wide). (c) HRCLS from the (9×9) surface oxide. The lines indicate calculated core level binding energies according to the model in figures 6(a) and (b).

and the p(2×1) [40] using moderate temperatures and pressures. At slightly higher coverages and temperatures, $(2\sqrt{3} \times 2\sqrt{3})$R30° and a p$(2 \times 2)$-3O structures are formed, as have been described elsewhere [41]. Early studies indicated that additional structures exist at even higher oxygen exposures on the Rh(111) surface [42]; however, the atomic arrangement was never studied in detail.

The surface oxide on Rh(111) is formed at a temperature of 750 K and using an O_2 partial pressure of 5×10^{-4} mbar, resulting in the LEED pattern as shown in figure 5(a) [13]. The periodicity of the oxygen-induced hexagonal pattern is close to a (9×9). One straightforward interpretation of the pattern is a moiré pattern consisting of a hexagonal layer with a larger in-plane lattice distance being on top of the hexagonal (111) surface layer. Thus, the moiré pattern comes about by the coincidence lattice between the two layers, and the in-plane distance in the overlayer can be estimated to be approximately 3 Å. This distance can be measured more precisely by the use of SXRD. The (9×9) induced peak found at -0.89 reciprocal lattice units yields directly a lattice distance in the oxygen-induced overlayer of 3.02 Å, in good agreement with the LEED observation.

The observations by diffraction are directly confirmed by STM. In figure 5(b), an STM image displaying bright protrusions in the surface oxide can be seen, as well as a long-range undulation induced by the coincidence between the lattice of the Rh oxide and that of the Rh(111) surface resulting in a moiré pattern. By observing that the periodicity of the moiré pattern can be described by around 7–8 of the overlayer unit-cells, we find also by this technique an in-plane lattice distance in the surface oxide of around 3 Å.

Turning to the HRCLS measurements to explore the chemical composition of the surface oxide, the O 1s and Rh $3d_{5/2}$ components from the (9×9) surface oxide are shown in figure 5(c). Starting with the O 1s region, two components with about equal intensities can clearly be discriminated. This strongly indicates that the surface oxide consists of two distinct Rh coordinated O species in equal amounts. By performing energy dependent measurements, the component with the higher binding energy can be shown to be closer to the bulk as compared to the other. Further, in the Rh $3d_{5/2}$ region, one highly O coordinated Rh species (307.9 eV) can easily be observed. It should be noted that the intensities of the various components are strongly influenced by the coexistence of other oxygen-induced structures on the surface, making the preparation procedure of the (9×9) structure of utmost importance for

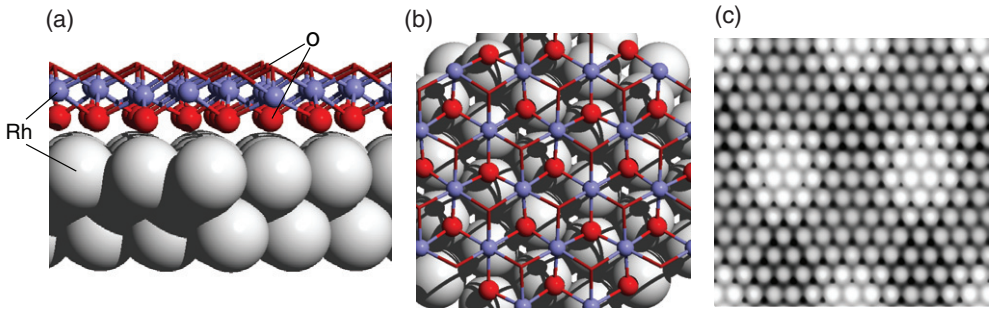

Figure 6. (a) Side view and (b) top view of the (9 × 9) structure as obtained by DFT. To avoid overcrowding the topmost O atoms are not shown as balls. (c) Simulated STM image from the model in (a).

a correct interpretation. If the sample preparation is done with care, we find a close to 1:1 ratio between the two O 1s components and a 8:9 ratio between the highly oxygen coordinated Rh species and the surface component of the clean surface. Assuming that the number of O atoms giving rise to one O component equals that of the number of Rh atoms in the highly oxygen coordinated Rh $3d_{5/2}$ component, we find a Rh coverage of approximately 0.9 and thus a total oxygen coverage of 1.8 ML. Thus, all qualitative measurements indicate a layered O–Rh–O surface oxide.

In order to calculate the structure of the surface oxide on Rh(111) the starting point was to simulate the termination of a bulk corundum $Rh_2O_3(0001)$ surface. The calculations show that the bulk terminated structure $O_3Rh_2O_3Rh_2$ reconstructs into $O_3Rh_3O_3Rh_1$, which is the most stable termination, and is terminated by a O–Rh–O trilayer. Therefore, the in-plane lattice distance of a free-standing O–Rh–O trilayer was calculated, and a value of 3.10 Å could be found. By comparing this to the calculated in-plane lattice distance 2.72 Å of Rh(111) a ratio of 7/8 is found. By relaxing the complete (7 × 7) cell on an (8 × 8) Rh(111) cell, the structure as shown in figure 6(a) is found. This is in slight disagreement with what is found using SXRD; however, in DFT, the (7 × 7) on an (8 × 8) is almost degenerate with an (8 × 8) on a (9 × 9).

To confirm the structure obtained for this particular surface oxide, we have simulated the STM image as shown in figure 6(c). Here it is interesting to note that the protrusions correspond to O atoms, which normally are considered to be imaged as depressions in STM. Further, the calculated core level binding energies agree well with the measured values, as shown in figure 5(c) [13].

The reduction of the (9 × 9) by CO using a CO partial pressure of 2×10^{-8} mbar at 375 K was studied *in situ* using HRCLS, STM and DFT [44]. It could be shown that despite the fact that CO does not adsorb easily on the (9 × 9) at these temperatures and pressures, the (9 × 9) surface oxide could be reduced. Interestingly, both HRCLS and STM showed that atomic oxygen was expelled from the (9 × 9) onto the reduced, metallic areas. DFT could explain these observations, since the O/Rh(111) phase diagram indicated that the (9 × 9) is not stable if the surrounding metal is free of atomic O. Therefore the (9 × 9) will decompose and act as an additional source of oxygen for the CO oxidation reaction on the metal surface. The (9 × 9) surface oxide can be also reduced by hydrogen. Similar to the case of CO, the surface oxide is inert with respect to H_2 adsorption, and the reduction speed increases significantly as soon as sizeable reduced areas become available for H_2 adsorption. During the later stages of adsorption, the reaction takes place at the boundary line between the surface oxide and the reduced area and limits the reduction rate [45].

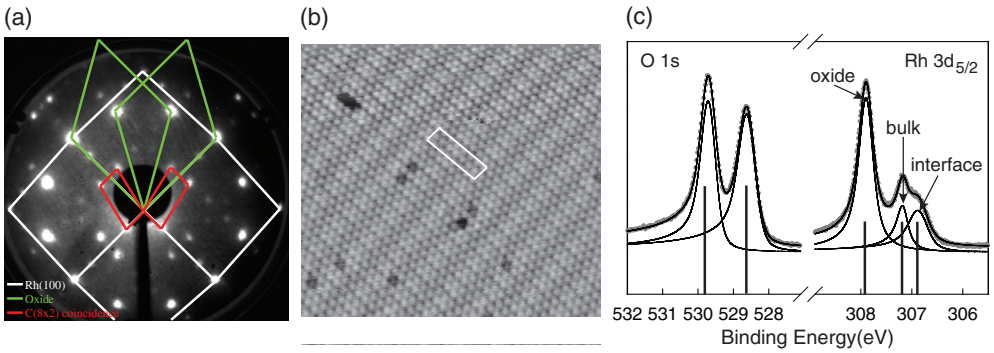

Figure 7. (a) LEED pattern from the Rh(100) surface after 5×10^{-5} mbar O_2 for 600 s at 700 K. The c(8 × 2) unit cell as well as the hexagonal cell is indicated. (b) STM image from the c(8 × 2) on Rh(100) (100 Å wide, $U = -0.11$ V and $I = 1$ nA). The c(8 × 2) unit cell is indicated. (c) HRCLS from the c(8 × 2) on Rh(100). The black vertical lines indicate calculated core level energies according to the model in figure 8(a).

3.4. Surface oxide on Rh(100): c(8 × 2)

Extensive studies have been performed of the O/Rh(100) systems previously [43, 46–50]. The best documented superstructures are the p(2 × 2) at a coverage of $\theta = 1/4$ ML, and a c(2 × 2) at $\theta = 1/4$–$1/2$ ML, as well as a p(2 × 2) with pg symmetry at a coverage of exactly $\theta = 1/2$ ML. Very early studies showed the existence of a p(3 × 1) structure and a c(8 × 2) structure [51].

The LEED pattern resulting from the formation of a surface oxide on this surface is shown in figure 7(a) [23]. By close inspection it can be shown that this pattern has indeed a c(8 × 2) periodicity. It is also clear from the pattern that a dominating feature is a hexagonal structure, yielding an in-plane lattice distance of approximately 3.07 Å. Thus, the LEED pattern indicates a commensurate structure with an internal hexagonal structure, the surface oxide, on top of a square structure, the Rh(100) substrate.

The STM measurements directly confirm the LEED observations. The high-resolution STM image shown in figure 7(b) immediately confirms the hexagonal structure of the surface oxide, as well as the more long range undulation due to the surface oxide/substrate interface structure. By counting the number of oxide lattice distances and using the moiré formula, it can be shown from the image that seven surface oxide interatomic distances correspond to eight substrate distances, resulting in a in-plane lattice distance of 3.07 Å, exactly as obtained from the LEED pattern.

Turning to the HRCLS measurements, again we find two components in the O 1s and a Rh $3d_{5/2}$ component corresponding to highly oxygen coordinated Rh as well as an interface peak; see figure 7(c). By using the expected O coverages of 0.25 and 0.5 ML from the p(2 × 2) and the p2g, respectively, we may estimate that the O coverage in the c(8 × 2) structure is 1.7 ML. Further, by using the intensity of the surface component from the clean surface we may estimate the Rh coverage due to the highly oxygen coordinated Rh to be slightly less than 1 ML.

The experimental data as obtained from LEED, STM and HRCLS immediately indicate a similar O–Rh–O trilayer surface oxide as observed on Rh(111). Thus, it is straightforward to propose a model, which may be tested in DFT. The resulting structure is shown in figures 8(a) and (b) and the simulated STM image and calculated core level binding energies are shown in figures 8(c) and 7(c), respectively. The agreement between theory and experiment is in

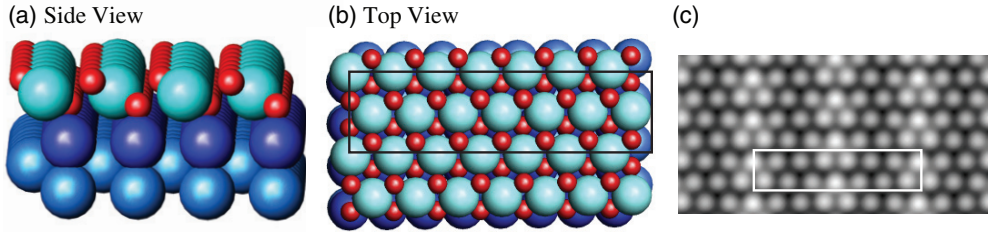

Figure 8. (a) Side-view and (b) top-view of the c(8 × 2) structure on Rh(100) as obtained by DFT. (c) Simulated STM image from the model in (a).

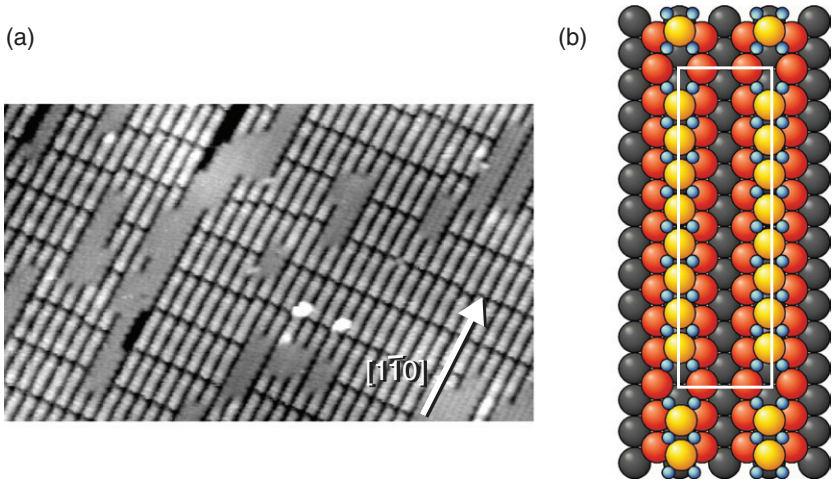

Figure 9. (a) STM image (400 Å wide, $I = 1$ nA, $V = 0.6$ V) from the Rh(110) surface after exposure to moderate pressures of O_2 and subsequent annealing. (b) Model of the (10 × 2) reconstruction. From [24, 53].

this case excellent. The structure was also determined by quantitative LEED and quantitative SXRD, removing all doubts about the structure of the O–Rh–O trilayer surface oxide on Rh(100) [23].

4. Other surface oxides

4.1. Surface oxides on Rh(110)

Oxygen adsorption on the Rh(110) surface results in a number of oxygen-induced structures [52]. Upon moderate oxygen exposures and subsequent heating, a (10 × 2) reconstruction can be observed in LEED. In figure 9(a) an STM image from this structure is shown. It can be seen that the structure is segmented in the [1$\bar{1}$0] direction. This structure is similar to the (12 × 2) structure on Pt(110) (see below). In addition, a distinct binding energy shift of the O 1s level towards lower binding energy can be seen between the so-called (2 × 2)$p2mg$ and the (10 × 2) structure [53]. A model of the structure is shown in figure 9(b), and it can be seen that the structure is a mixture of reconstructed Rh(110)-(2 × 1) and unreconstructed areas [24, 53]. The nearest neighbour distance along the ridges in the

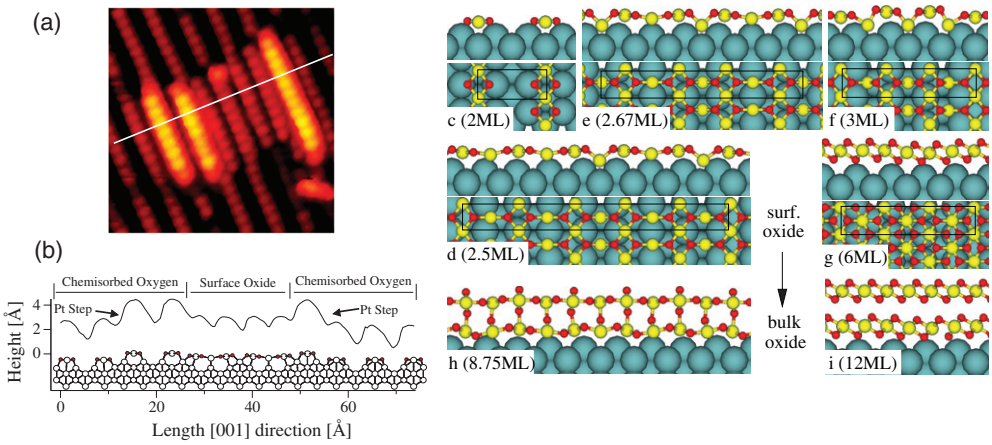

Figure 10. (a) STM image 46 Å wide, $I = 1.5$–2 nA, $V = 1$–1.75 V from the Pt(110) surface after exposure to atomic O. (b) Line scan along the white line in (a) and a model based on DFT calculations. ((c)–(i)) Models of the one-dimensional oxide (c), surface oxide ((d), (f)) and thicker oxide structures ((g)–(i)). ML refers to one monolayer being equal to the number of Pt atoms in the Pt(110)-(1 × 2) surface layer. O atoms are small and dark (red), Pt atoms in the oxide are small and bright (yellow) and substrate Pt atoms are shown as large balls (blue). From [22].

[1$\bar{1}$0] direction are expanded by approximately 10%, yielding a lattice distance of 3 Å, close to the Rh distances in the surface oxides observed on Rh(111) and Rh(100) as described above. Since the O atoms flanking the uppermost Rh row have the same interatomic distance, a value typical for O–O distances in transition metal oxides [54], one can consider this structure a one-dimensional oxide, consisting of the topmost Rh row and its O neighbours. A similar structure was also found along the steps of a vicinal Rh surface [55].

Exposing the Rh(110) surface to O pressures of around 1×10^{-4} mbar at 750 K, a well-ordered thin oxide film can be formed [56]. The LEED pattern displays a c(2 × 4) pattern with brighter hexagonally arranged spots. The highly resolved STM images shows a quasi-hexagonal arrangement of the top oxygen atoms of the oxide film. Furthermore, the O 1s and Rh $3d_{5/2}$ HRCLS spectra from the c(4 × 2)oxide film on the Rh(110) surface are very similar to those reported for the surface oxide on the Rh(111) and Rh(100) surfaces as described above. The structural model of this surface oxide, based on a detailed LEED, STM, HRCLS and DFT study, will be reported [57]. In short, the surface oxide grown on the Rh(110) surface resembles the structure of those formed on the Rh(111) and Rh(100) surfaces and can be described in terms of an O–Rh–O trilayer.

In the presence of potassium, it was found that growth of both the one-dimensional oxide and the trilayer oxide needs significantly lower oxygen doses than on the pure Rh(110) surface. It was concluded that K facilitates dissociation of O_2 by its mere presence on the surface, but also by stabilizing a more open surface structure [58].

4.2. Surface oxides on Pt(110)

The existence of a surface oxide on Pt(110) was recently shown by combining STM, temperature programmed desorption (TPD) and DFT [22]. In that case, high oxygen coverages were achieved either by high-pressure O_2 exposures in a dedicated high-pressure cell at a temperature of 500 K or by dosing atomic oxygen, resulting in a surface imaged with STM as shown in figure 10(a). The phase displaying large domains on the surface could be shown

to be a structure built from ($n \times 2$) units, where n is peaked at 12, and therefore was denoted a (12 × 2) structure [59, 60]. The Pt–Pt distance in the rows along the ridges in the [1$\bar{1}$0] direction has been expanded by 9% in conjunction with the adsorption of 22 O atoms in each stripe. Thus, the Pt atoms along the ridges in the Pt(110) surface are each coordinated to four O atoms (see figure 10(c)), and essentially the same structure as the one-dimensional (10 × 2) oxide on Rh(110) develops. The different periodicity can be easily rationalized by the larger lattice constant of Pt. An O–O distance along the rows of approximately 3 Å can be achieved by either placing 9 O atoms on 10 Rh–Rh interatomic distances ($d_{O-O} = 2.99$ Å) or 11 O atoms on 12 Pt–Pt interatomic distances ($d_{O-O} = 3.03$ Å). As on Rh, a one-dimensional oxide similar to that on the (110) surface also forms along the steps of a vicinal Pt surface. This one-dimensional oxide is highly reactive in CO oxidation [61], similar to that on Pt(110) [62].

When forming the (12 × 2) one-dimensional oxide, because of the expansion, some Pt atoms are expelled onto the surface and reoxidize to form more densely packed surface oxide layers. Larger areas of such structures were observed at higher oxygen coverage. A zoom-in on such an island, as shown in figure 10(a), reveals a strong compression in the [001] direction. Some rows within the islands are shifted by 1/4 of a row distance of the (12 × 2) in the [001] direction. In addition, a 29% compression in the [001] direction is found for the less protruding stripes in the island. Thus, these shifted and compressed stripes are associated to the formation of a two-dimensional surface oxide. The DFT calculations support the experimental observations; the structure of the one-dimensional (12 × 2) and the two-dimensional surface oxide is shown at the bottom in figure 10(b) together with a line scan from the STM image in figure 10(a). Extensive DFT calculations were performed with respect to stable structures as the oxygen coverage is increasing, as shown in figures 10(c)–(i). It is interesting to note that the two-dimensional structures on Pt in figures 10(d)–(f) are essentially buckled versions of the PdO(101) structure observed on Pd(100), a similarity related to the fact that PtO and PdO have the same structure.

4.3. Oxygen on Ag(111) and Ag(100)

The interaction of oxygen with the Ag(111) surface has been studied intensively during the years; for a comprehensive review see [63]. The main reason is the importance of the partial oxidation of ethene to epoxide, which is catalysed by Ag. In contrast to Pd and Rh, the sticking probability of molecular oxygen with thermal energies is very low, even on clean Ag surfaces. For Ag(111) at 490 K, an initial sticking coefficient of approximately 10^{-7} has been reported [64]. Therefore, structures with high oxygen coverage on Ag(111) can be achieved only by either dosing at high pressure (mbar to bar range), using a molecular beam with higher kinetic energy of the O_2 molecules or using gases with higher oxidizing potential such as atomic oxygen or NO_2.

In particular a p(4 × 4) structure has been studied intensely: partly because the structure appears at conditions relevant for the oxidation of ethene, and partly because the structure was one of the first phases considered a surface oxide [63, 65]. In two recent articles the p(4 × 4) structure has been determined independently [66, 67]. The original reason for the renewed interest in the p(4 × 4) was the observation that quantitative SXRD data [66] could not be reproduced by any of the previously existing models [63]. Here, the data are presented as in the article by Schmid *et al* [66]; however, the final structure is the same as the one found by Schnadt *et al* [67].

In figure 11(a) the LEED pattern after oxidation of Ag(111) by NO_2 is shown, and the p(4 × 4) superstructure can be seen. The corresponding STM image recorded at room

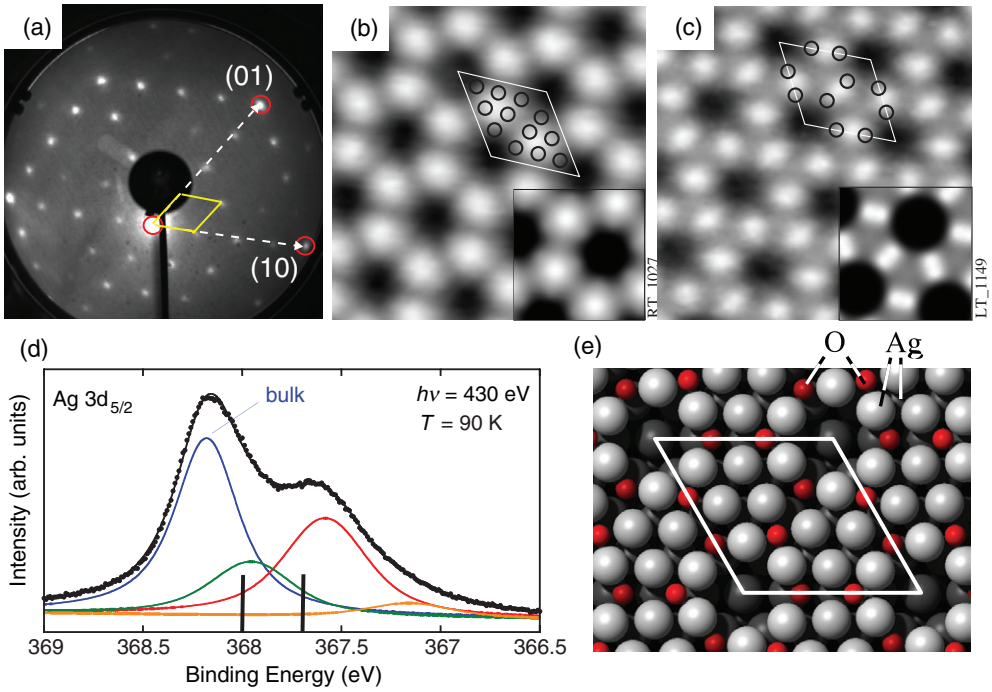

Figure 11. (a) The p(4 × 4) oxygen-induced LEED pattern on Ag(111). (b) STM images of the oxygen-induced p(4 × 4) structure on Ag(111) recorded at RT and (c) at liquid nitrogen (80 K) temperature. The insets show simulated images [66] and the small black circles mark the positions of the Ag and O atoms, respectively. (d) Photoemission spectrum of the Ag $3d_{5/2}$ level. The black lines indicate calculated binding energies. (e) Model for the p(4 × 4) structure.

temperature is shown in figure 11(b), displaying a honeycomb structure known already from previous studies [68]. At 80 K and similar tunnelling conditions, protrusions at the positions between the minima in the honeycomb images can be seen (figure 11(c)). The only feature present in all images is the 'corner hole' appearing up to approximately 2 Å deep. To determine the number of Ag atoms in the unit cell, the structure was reduced by CO and the amount of remaining metallic Ag was determined. After the reduction, we find that CO-induced holes amount to approximately 25% of the area after reduction. Since the reduced Ag(111) surface contains 16 Ag atoms in the area of the p(4 × 4) cell, this means that the p(4 × 4) phase contains 12 ± 1 Ag atoms in its unit cell. From this information, the structure model shown in figure 11(e) emerges. The Ag atoms are arranged in two Ag_6 triangles, one triangle in fcc sites and the other in hcp sites of the substrate, all with metallic Ag–Ag distances. The O atoms are in four-fold hollow sites in the furrows between the triangles, leaving the corner hole empty. The position of the O atoms also explains the protrusions sometimes seen by STM at low temperatures (figure 11(c)).

Turning to HRCLS, the O 1s signal from the p(4 × 4) displays a single component (not shown), indicating only a single O species on the surface. For Ag $3d_{5/2}$, as shown in figure 11(d), a deconvolution of the experimental spectra shows three peaks with lower binding energy than the bulk; the strongest ones are at approximately −0.60 and −0.23 eV. The component with the larger shift can be attributed to the Ag atoms at the sides and the corners of the Ag triangles in the model in figure 11(e), while the component with the smaller shift is due Ag atoms at the bottom of the furrow between the triangles, below the O atoms. The HRCLS

measurements therefore confirm the model in figure 11(e). Furthermore, the experimental structure factors from SXRD measurements could be reproduced by this model [66].

It is interesting to note that in spite of compelling experimental evidence for our model of the p(4 × 4) phase as presented above, it does not have the lowest energy of all models [63] in well-converged DFT calculations. At present, this fact is attributed to a problem of today's semi-local functionals, which do not take the van der Waals interactions between the closed 4d shells of Ag into account [66].

Whereas oxygen forms well-ordered p(2 × 2) overlayers on the (100) surfaces of most face-centred cubic metals, Ag(100) is an exception. The only reasonably well-ordered oxygen overlayer structure reported so far is a c(4×6) structure at an oxygen coverage of $\theta = 1/3$ [69]. An oxygen-induced c(2 × 2) structure found on this surface has been suggested to be actually a missing-row reconstruction [70]. Although DFT calculations predict an energy gain by a missing-row reconstruction, there are still many open questions concerning this system [71]. Furthermore, a p(6 × 6) phase has been observed, but its structure is unresolved so far and it is completely unclear whether it should be considered a reconstruction of the metal lattice or a surface oxide [69].

5. Summary and outlook

Less than five years after the first complete structural characterization of a surface oxide that differs from bulk oxides [19], and in spite of intensive research in that field, we are still far from a complete overview of the structural variety of surface oxides on the late transition metals. This is true even if we restrict ourselves to the two elements studied most thoroughly so far, Rh and Pd. As an example, a (surface) oxide is known to exist on Pd(110) [72], but no structural information is available. Concerning the 5d metals, structural studies of surface oxides are even more limited, being essentially restricted to the Pt(110) surface. It is quite certain that far more surface oxides exist on these metals, and it is quite likely that even Au(111), the most inert of all surfaces, can host a surface oxide, as indicated by the observation of a moiré structure on oxidized Au(111) [73]. For most surfaces studied so far, only one type of surface oxide was found. Only the future can tell whether this will be the rule.

In spite of the limitations of the data currently available, as a summary some common features and motifs as well as differences in the surface oxide structures should be noted. We will start by comparing the surface oxides observed so far to the bulk oxides of the respective metals.

Rh forms trilayer O–Rh–O oxides with hexagonal layers, which differ from the Rh_2O_3 bulk structure mainly by a complete filling of the octahedral sites of the oxygen lattice by Rh in the surface oxide, whereas only 2/3 of these sites are occupied in bulk Rh_2O_3. With its three-dimensional close-packed oxygen lattice and O–O distances of approximately 3 Å, the Rh surface oxides follow the same building rules as most transition metal oxides.

Pd forms essentially planar surface oxides, but with some buckling of the O lattice. In all of these structures, the oxygen atoms form a roughly square lattice, and the Pd atoms are distributed between them, with either two-fold or four-fold coordination. The stoichiometry of these structures lies in a narrow range between Pd_5O_4 and PdO. Also the surface oxides of Pd share some of the structural features of the corresponding bulk oxide PdO, which is characterized by a roughly simple-cubic oxygen lattice and Pd atoms with four-fold coordination to oxygen. PtO has the same structure as PdO, and also the planar surface oxides of Pt found so far are essentially the same as found on Pd surfaces.

The oxygen-induced structures of Ag known today, including the p(4 × 4) phase, cannot be considered true surface oxides since they are characterized by metal-like Ag–Ag distances.

In this respect, one should keep in mind, however, that also the most common silver oxide, Ag_2O, with its cuprite structure, does not abide by the building rules of most other transition metal oxides [54]. With its 20% dilated fcc metal lattice and extremely large O–O distances of 4.1 Å in Ag_2O, the cuprite structure can be considered an fcc metal with oxygen dissolved in tetrahedral sites[5], thus also here it is the metal lattice that dictates the structure, not the oxygen lattice, which determines the structure of the other transition metal oxides. Thus it is not astonishing that no 'true' surface oxides of Ag have been found so far.

With the exception of the one-dimensional oxides found at steps of vicinal surfaces and the ridges of the $(n \times 2)$-reconstructed (110) surfaces, all true surface oxides are thus characterized by an oxygen lattice equivalent to that in the respective bulk oxides, and metal atoms distributed in between in a fashion resembling more or less that of the bulk oxides. A structure mainly determined by the oxygen lattice, with more flexibility for the metal atoms, is also a common building principle of most bulk oxides, and many of these oxides are characterized by close-packed O lattices with O–O distances of approximately 3 Å, a value also typical for the surface oxides. It should be noted, however, that surface oxides do not necessarily follow this rule. The structure of alumina on NiAl(110) with oxygen at the surface forming triangular and square units, in contrast to the hexagonally close-packed O lattice planes in the bulk of all alumina structures, is a clear exception from this rule [74].

A further common feature of many surface oxides lies in their registry with respect to the substrate lattice. In contrast to adsorbed oxygen, which prefers hollow sites (fcc hollow sites on (111) surface), the surface oxides get their strongest bonding to the substrate if oxygen is placed in on-top positions of the substrate lattice, sometimes resulting in an alignment of the O rows of the surface oxide with close-packed rows of the substrate [13, 19, 23]. Although the oxides of the late transition metals are not very ionic, in this respect they behave like ionic crystals which bind to electropositive substrate atoms by their anions.

With respect to reactivity, similar to many bulk oxides, surface oxides terminated by a close-packed oxygen layer are essentially inert because they do not provide adsorption sites for reactants. These structures are attacked by reducing adsorbates such as CO and H_2 only at their borders [44, 45, 62]. Thus, once covered by a complete layer of such a surface oxide, single crystals will be much less reactive than small particles, which always exhibit structural defects of the oxides at edges and corners. As soon as part of the surface gets reduced, the reducing adsorbate can bind to the metal. In equilibrium, on all surfaces where data are available, the surface oxide does not coexist with the pure metal but rather with a significant concentration of adsorbed oxygen, which is the active phase for, for example, CO oxidation [44]. If the temperature is low enough, dissolution of the surface oxide at its borders will be too slow to provide oxygen for forming an adatom phase, however, and the reaction takes place immediately at the border of the oxide, which may be highly reactive [45, 75]. In both of these mechanisms, the surface oxide should be seen as a source of oxygen for the reaction. This is in contrast to oxides that exhibit catalytically active surfaces, such as the one-dimensional oxides [61, 62] present on the (110) and vicinal surfaces, presumably also on the edges of small particles of real-world catalysts, and oxides with coordinatively unsaturated metal atoms at the surface [3, 18].

In summary, the results presented in this report demonstrate the existence of surface oxides on late transition metals. In some cases, these phases, which are obviously different from O adatoms and have a high oxygen coverage, were previously explained as subsurface oxygen, a notion invalidated by the current results. Surface oxides are thin oxide layers, which represent a

[5] It should be noted that the stable site for single oxygen atoms in fcc Ag is the octahedral site, not the tetrahedral site as in Ag_2O [71, 76].

phase that is in between chemisorbed oxygen (adatoms) and the formation of the corresponding bulk oxide. A complete information on the atomic arrangement of the surface oxides layers is crucial for a full understanding of their properties. The review shows that a combination of experimental and theoretical techniques is essential in order to achieve the atomic-scale understanding. In particular, the development of theoretical techniques has greatly contributed to the present ability to solve highly complicated surface structures. At present, a concerted international effort is being carried out to increase the knowledge concerning the properties of these surface oxides.

Acknowledgments

This work was financially supported by the Swedish Research Council, the Crafoord foundation, the Knut and Alice Wallenberg foundation, the Austrian *Fonds zur Förderung der wissenschaftlichen Forschung*, and the European Union under contract no. NMP3-CT-2003-505670 (NANO2). Support by the MAX-lab and ESRF staff is gratefully acknowledged. The authors wish to thank J Gustafson, M Borg, A Resta, R Westerström, N Kasper, A Stierle, H Dosch, M Todorova, J Rogal, K Reuter, M Scheffler, X Torrelles, C Quiros, J Yuhara, L Köhler, C Klein, W Hofer, M De Santis, Y Gauthier, and C Konvicka for experimental and theoretical support as well as for stimulating discussions. J Schnadt is acknowledged for carefully reading the manuscript. Special thanks go to G Comelli, A Michaelides, and B Hammer for providing figures of the surface oxides on Rh(110), Ag(111) and Pt(110).

References

[1] Duke C B and Plummer E W (ed) 2001 Frontiers in surface and interface science *Surf. Sci.* **500** 1 (Special issue)
[2] Ertl G, Knözinger H and Weitkamp J 1997 *Handbook of Heterogeneous Catalysis* (New York: Wiley)
[3] Over H, Kim Y D, Seitsonen A P, Wendt S, Lundgren E, Schmid M, Varga P, Morgante A and Ertl G 2000 *Science* **287** 1474
[4] Hendriksen B L M and Frenken J W M 2002 *Phys. Rev. Lett.* **89** 046101
[5] Hendriksen B L M and Frenken J W M 2004 *Surf. Sci.* **552** 229
[6] Ackermann M D, Pedersen T M, Hendriksen B L M, Robach O, Bobaru S C, Popa I, Quiros C, Kim H, Hammer B, Ferrer S and Frenken J W M 2005 *Phys. Rev. Lett.* **95** 255505
[7] Freund H J, Kuhlenbeck H, Libuda J, Rupprechter G, Bäumer M and Hamann H 2001 *Top. Catal.* **15** 201
[8] Vestergaard E K, Thostrup P, An T, Lægsgaard E, Stensgaard I, Hammer B and Besenbacher F 2002 *Phys. Rev. Lett.* **88** 259601
[9] Peters K F, Walker C J, Steadman P, Robach O, Isern H and Ferrer S 2001 *Phys. Rev. Lett.* **86** 5325
[10] Rupprechter G, Dellwig T, Unterhalt H and Freund H J 2001 *J. Phys. Chem.* B **105** 3797
[11] Hansen P L, Wagner J B, Helveg S, Rostrup-Nielsen J R, Clausen H and Topsøe B S 2002 *Science* **295** 2053
[12] Lundgren E, Gustafson J, Mikkelsen A, Andersen J N, Stierle A, Dosch H, Todorova M, Rogal J, Reuter K and Scheffler M 2004 *Phys. Rev. Lett.* **92** 046101
[13] Gustafson J, Mikkelsen A, Borg M, Lundgren E, Köhler L, Kresse G, Schmid M, Varga P, Torrelles X, Quiros C and Andersen J N 2004 *Phys. Rev. Lett.* **92** 46101
[14] He Y B, Knapp M, Lundgren E and Over H 2005 *J. Phys. Chem.* B **109** 21825
[15] Stierle A, Kasper N, Dosch H, Gustafson J, Mikkelsen A, Andersen J N and Lundgren E 2005 *J. Chem. Phys.* B **122** 44706
[16] Ketteler G, Ogletree D F, Bluhm H, Liu H J, Hebenstreit E L D and Salmeron M 2005 *J. Am. Chem. Soc.* **127** 18269
[17] Schalow T, Laurin M, Brandt B, Schauermann S, Guimond S, Kuhlenbeck H, Starr D E, Shaikhutdinov S K, Libuda J and Freund H J 2005 *Angew. Chem. Int. Edn* **44** 7601
[18] Over H, Seitsonen A P, Lundgren E, Schmid M and Varga P 2001 *J. Am. Chem. Soc.* **123** 11807
[19] Lundgren E, Kresse G, Klein C, Borg M, Andersen J N, De Santis M, Gauthier Y, Konvicka C, Schmid M and Varga P 2002 *Phys. Rev. Lett.* **88** 246103
[20] Reuter K and Scheffler M 2003 *Phys. Rev. Lett.* **90** 046103
[21] Todorova M *et al* 2003 *Surf. Sci.* **541** 101

[22] Li W X, Österlund L, Vestergaard E K, Vang R T, Matthiesen J, Pedersen T M, Lægsgaard E, Hammer B and Besenbacher F 2004 *Phys. Rev. Lett.* **93** 146104
[23] Gustafson J *et al* 2005 *Phys. Rev.* B **71** 115442
[24] Africh C, Esch F, Li W X, Corso M, Hammer B, Rosei R and Comelli G 2004 *Phys. Rev. Lett.* **93** 126104
[25] Kresse G, Lundgren E, Bergermayer W, Podloucky R, Koller R, Schmid M and Varga P 2003 *Appl. Phys.* A **76** 701
[26] Tersoff J and Hamann D R 1985 *Phys. Rev.* B **31** 805
[27] Conrad H, Ertl G, Küppers J and Latta E E 1977 *Surf. Sci.* **65** 245
[28] Zheng G and Altman E I 2000 *Surf. Sci.* **462** 151
[29] Gabasch H, Unterberger W, Hayek K, Klötzer B, Kresse G, Klein C, Schmid M and Varga P 2006 *Surf. Sci.* **600** 617
[30] Klikovits J *et al* 2006 to be published
[31] Orent T W and Bader S D 1982 *Surf. Sci.* **115** 323
[32] Stuve E M, Madix R J and Brundle C R 1984 *Surf. Sci.* **146** 155
[33] Chang S-L and Thiel P A 1988 *J. Chem. Phys.* **88** 2071
[34] Chang S-L, Thiel P A and Evans J W 1988 *Surf. Sci.* **205** 117
[35] Zheng G and Altman E I 2002 *Surf. Sci.* **504** 253
[36] Rieder K H and Stocker W 1985 *Surf. Sci.* **150** 66
[37] Vu D T, Mitchell K A R, Warren O L and Thiel P A 1994 *Surf. Sci.* **318** 129
[38] Saidy M, Warren O L, Thiel P A and Mitchell K A R 2001 *Surf. Sci.* **494** L799
[39] Kostelnik P *et al* 2006 to be published
[40] Ganduglia-Pirovano M V, Scheffler M, Baraldi A, Lizzit S, Comelli G, Paolucci G and Rosei R 2001 *Phys. Rev.* B **63** 205415
[41] Köhler L, Kresse G, Lundgren E, Schmid M, Gustafson J, Mikkelsen A, Borg M, Yuhara J, Andersen J N and Varga P 2004 *Phys. Rev. Lett.* **93** 266103
[42] Logan A D, Datye A K and Houston J E 1991 *Surf. Sci.* **245** 280
[43] Mercer J R, Finetti P, Scantlebury M J, Beierlein U, Dhanak V R and McGrath R 1997 *Phys. Rev.* B **55** 10014
[44] Lundgren E *et al* 2005 *J. Electron Spectrosc. Relat. Phenom.* **144** 367
[45] Klikovits J, Schmid M, Gustafson J, Mikkelsen A, Resta A, Lundgren E, Andersen J N and Varga P 2006 *J. Phys. Chem.* B **110** 9966
[46] Baraldi A, Dhanak V R, Comelli G, Prince K C and Rosei R 1997 *Phys. Rev.* B **56** 10511
[47] Shen Y G, Qayyum A, O'Connor D J and King B V 1998 *Phys. Rev.* B **58** 10025
[48] Alfe D, de Gironcoli S and Baroni S 1998 *Surf. Sci.* **410** 151
Alfe D, de Gironcoli S and Baroni S 1999 *Surf. Sci.* **437** 18
[49] Baraldi A, Cerda J, Martyn-Gago J A, Comelli G, Lizzit S, Paolucci G and Rosei R 1999 *Phys. Rev. Lett.* **82** 4874
[50] Norris A G, Schedin F, Thornton G, Dhanak V R, Turner T S and McGrath R 2000 *Phys. Rev.* B **62** 2113
[51] Tucker C W 1966 *J. Appl. Phys.* **37** 3013
[52] Comelli G, Dhanak V R, Kiskinova M, Prince K C and Rosei R 1998 *Surf. Sci. Rep.* **32** 165
[53] Vesselli E, Africh C, Baraldi A, Comelli G, Esch F and Rosei R 2001 *J. Chem. Phys.* **114** 4221
[54] Cox P A 1992 *Transition Metal Oxides* (Oxford: Clarendon)
[55] Gustafson J *et al* 2006 *Phys. Rev.* B at press
[56] Dudin P, Barinov A, Gregoratti L, Kiskinova M, Esch F, Dri C, Africh C and Comelli G 2005 *J. Phys. Chem.* B **109** 13649
[57] Dri C, Africh C, Esch F, Comelli G, Dubay O, Köhler L, Mittendorfer F, Kresse G, Dudin P and Kiskinova M 2006 submitted
[58] Günther S, Esch F, del Turco M, Africh C, Comelli G and Kiskinova M 2005 *J. Phys. Chem.* B **109** 11980
[59] Helveg S, Lorensen H T, Horch S, Lægsgaard E, Stensgaard I, Jacobsen K W, Nørskov J K and Besenbacher F 1999 *Surf. Sci.* **430** L533
[60] Walker A V and King D A 1998 *J. Chem. Phys.* **109** 6879
[61] Wang J G *et al* 2005 *Phys. Rev. Lett.* **95** 256102
[62] Pedersen T M, Li W X and Hammer B 2006 *Phys. Chem. Chem. Phys.* **8** 1566
[63] Michaelides A, Reuter K and Scheffler M 2005 *J. Vac. Sci. Technol.* A **23** 1487
[64] C T Campbell 1985 *Surf. Sci.* **157** 43
[65] Rovida G, Pratesi F, Maglietta M and Ferroni E 1974 *Surf. Sci.* **43** 230
[66] Schmid M *et al* 2006 *Phys. Rev. Lett.* **96** 146102
[67] Schnadt J, Michaelides A, Knudsen J, Vang R T, Reuter K, Lægsgaard E, Scheffler M and Besenbacher F 2006 *Phys. Rev. Lett.* **96** 146101
[68] Carlisle C I, King D A, Bocquet M-L, Cerda J and Sautet P 2000 *Phys. Rev. Lett.* **84** 3899

[69] Costina I, Schmid M, Schiechl H, Gajdoš M, Stierle A, Kumaragurubaran S, Hafner J, Dosch H and Varga P 2006 *Surf. Sci.* **600** 617
[70] Rocca M *et al* 2000 *Phys. Rev.* B **61** 213
[71] Gajdoš M, Eichler A and Hafner J 2003 *Surf. Sci.* **531** 272
[72] Bondzie V A, Kleban P and Dwyer D J 1996 *Surf. Sci.* **347** 319
[73] Chevrier J, Huang L, Zeppenfeld P and Comsa G 1996 *Surf. Sci.* **355** 1
[74] Kresse G, Schmid M, Napetschnig E, Shishkin M, Köhler L and Varga P 2005 *Science* **308** 1440
[75] Li W X and Hammer B 2005 *Chem. Phys. Lett.* **409** 1
[76] Crocombette J-P, de Monestrol H and Willaime F 2002 *Phys. Rev.* B **66** 024114